Semiconductor Experiment: Schottky Diode

Vinh Tran, Kam Modjtahedzadeh, Raza Kazmi

October 22, 2021

Abstract

We explored the current dependency on voltage and temperature of an Au-Si junction, an example of a rectifying Schottky diode, whose characteristic feature is the potential barrier formed at the interface between the metal and semiconductor. We performed current measurements in two stages: first at room temperature and second by varying the temperature of the diode using a closed cycle cryostat or physical property measurement system (PPMS). From thermionic emission theory, we predict the overall shape of the current curve to follow an exponential curve for positive bias and be flat for reverse bias. We find that the general behavior of the IV curve both agrees the predicted expression from thermal emission theory (TET) as voltage is varied for fixed temperature as well as demonstrating the expected decrease in current magnitude for lower temperatures save for an anomalous increase in the magnitude from 295 K to 255 K where the magnitude instead increases slightly. Using the framework of TET we were able to extract various parameters such as the Schottky barrier height of the sample which we find to be 0.3216 eV at -5V and 0.2833 eV at -3V.

1 Introduction

1.1 Energy Band Structure, Band Gaps, Metals and Semiconductors

Energy bands are the allowed energies as a function of wavevector k. Gaps in the energy band, or band gaps, will in general appear at the edges of unit cells in momentum space, the Brillouin zone [5, pg.]

The general concept of a band gap comes from treating electrons as free plane waves interacting in a periodic potential. That is, the Hamiltonian of the system takes the form

$$\hat{H} = \hat{H}_0 + \hat{V}(\vec{r}) = \frac{\hat{p}^2}{2m} + \hat{V}(\vec{r}) \qquad \hat{V}(\vec{r}) = \hat{V}(\vec{r} + \vec{R}) \tag{1}$$

where the energy eigenvalues of the free Hamiltonian, E_0 are

$$\hat{H}_0 \left|k\right\rangle = E_0 \left|k\right\rangle \qquad \left|k\right\rangle = e^{i\vec{k}\cdot\vec{r}} \qquad \text{and} \qquad E_0 = \frac{\hbar^2 |\vec{k}|^2}{2m} \tag{2}$$

Treating this periodic potential $V(r)$ as a perturbation to the free electron Hamiltonian $\hat{H}_0$, we can solve for the shifted energy eigenvalues using second order degenerate perturbation theory which yields the perturbed energies at the boundaries of the Brilluoin zones as

$$E_\pm = E_0 \pm |V_G| \qquad \text{where} \qquad V_G = \left\langle k' \right| \hat{H} \left|k\right\rangle \tag{3}$$

where $E_\pm$ are the shifted energies due to the periodic potential, E_0 are the unperturbed energies, and V_G as defined above is the matrix element of the full Hamiltonian $\hat{H}$ for states $\left|k\right\rangle, \left|k'\right\rangle$.

The effect of the periodic potential is then to lift the degeneracy and create a gap in the energy levels in an analagous manner to the splitting of energy levels in the Stark or Zeeman effect for the Hydrogen atom [5, pg. 166-167]. Moreover, expanding about the boundary, we get an expression for the allowed energies as a function of angle δ which describes the "position" in momentum space. In particular, in the reduced zone, we have energy as a function of angle from $-\pi/a$ to π/a where a is the lattice constant, m is the mass of the electron, and $\hbar$ is Planck's reduced constant.

$$E_\pm(\delta) = \frac{\hbar^2 (n\pi/a)^2}{2m} \pm |V_G| + \frac{\hbar^2 \delta^2}{2m}\left[1 \pm \frac{\hbar^2 (n\pi/a)^2}{m}\frac{1}{|V_G|}\right] \tag{4}$$

In particular, for the latter case, the result are parabolic bands [5, Ch. 15]

In the case of a metal, the "lower band" is only partially filled. As such, when a voltage is applied, electrons are free to move and conduct current. For a semiconductor on the other hand, the lower band is fully filled but the energy gap between the lower and upper band is of the order 4 eV or less. Thus, it is possible to excite electrons to cross from the lower band to the conduction band by supplying energy equal to the band gap.

1.2 Metal-Semiconductor Junction and Schottky Barrier

For the metal-semiconductor junction, in the case where the semiconductor is $n-$type doped, the band structure takes on a characteristic barrier at the metal-semiconductor interface, called the Schottky barrier, which gently slopes down towards the semiconductor side but is a steep jump on the metal side as visualized in Fig. 1. This shape determines the IV characteristic of the junction; electrons from the semiconductor side, with an applied voltage, can more easily flow over the barrier and continue onto the metal side. The barrier acts to prevent flow in the reverse direction, from the metal however.

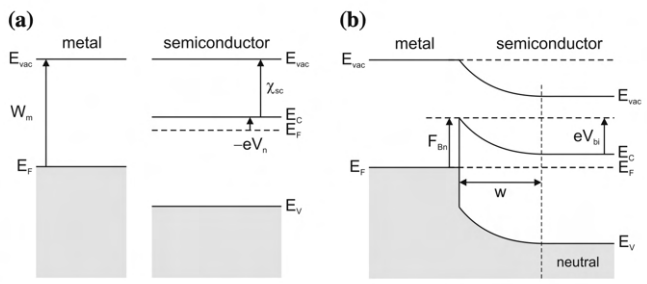

Fig. 21.3 Schematic band structure of a metal–semiconductor junction that is dominated by bulk properties of the semiconductor. (**a**) no contact, (**b**) metal and semiconductor in contact. w denotes the width of the depletion layer. Outside the depletion layer the semiconductor is neutral. $F_{B,n}$ denotes the Schottky barrier height, V_{bi} denotes the built-in voltage (here $V_{bi} > 0$)

Figure 1: Figure from Grundmann Physics of Semiconductors illustrating on the right the shape of the Schottky barrier and on the left the energy band structures in the case of a metal and semiconductor separately [1, pg. 598]

The mechanism behind the barrier formation depends on the fact that metals and semiconductors have different Fermi levels, that is, different chemical potentials. When the two are in contact, the Fermi level of the two reach a constant level for the whole system in thermal equilibrium. As a result, electrons will flow from the semiconductor to the metal which forms a potential barrier [1].

Then the Schottky barrier height $F_{Bn} = q\Phi_{Bn}$ [1] can be characterized by the difference in the metal work function W_m and the electron affinity χ of the semiconductor. The former is the chemical potential of electrons for the metal body $W_m = E_{\text{vac}} - E_F$ and the latter is defined as the difference between the energy of the vacuum level and the conduction band edge: $\chi = E_{\text{vac}} - E_C$ [1, pg. 586].

$$\boxed{q\Phi_{Bn} = W_m - \chi} \tag{5}$$

1.3 Thermionic Emission Model: Current Density as a function of T, V

One way electrons can flow from the semiconductor to the metal is to gain enough energy and go "above" the barrier (as opposed to tunneling through the barrier); this type of transport can be described by thermionic emission theory which calculates the current density j assuming that the velocities or equivalently the energies of the electrons are distributed according to the Maxwell-Boltzmann distribution [6, pg. 156].

The main result of the thermionic emission model is an expression for the current density as

$$\boxed{j = j_s \left[\exp\left(\frac{qV}{kT}\right) - 1 \right]} \tag{6}$$

[1] There appears to be some sort of conflicting notation between various texts. In some Φ is a voltage and thus $q\Phi$ is the barrier height, which has units of eV or energy. In other cases Φ refers to the barrier and has units of eV. Throughout the rest of this paper, we refer to $q\Phi_{Bn}$ as the barrier height.

with j_s the saturation current density being given by

$$j_s = A^* T^2 \exp\left(-\frac{q\Phi_{Bn}}{kT}\right) \tag{7}$$

where k is Boltzmann's constant, T is the temperature, q is the charge of the electron, and A^* is known as the Richardson constant given by

$$A^* = \frac{4\pi q m^* k^2}{h^3} = 120 \frac{\mathrm{A}}{\mathrm{cm^2 K^2}} \qquad \text{for} \qquad m^* = m_e \tag{8}$$

where m^* is the effective mass of the electron and h is Planck's constant. This constant appears from solving for the current density j in the process described below as a collection of coefficients that appear in front of the exponential term. Inserting for all known values and constants yields $A^* = 120$ A cm^{-2} K^{-2}.

The main steps of to arrive at this expression starts from a general expression for the current density as an integral over the number density of the electrons

$$j = \sum_i n_i q_i v_i = \int_{E_{\min}}^{\infty} (-e) v_x \, dn \tag{9}$$

and changing the variable of integration to incorporate the fact that the electrons are thermally excited and thus are distributed probabilistically so that we can re-write $dn = D(E) f(E) \, dE$ where $D(E)$ is the density of states of the electrons and $f(E)$ is the Maxwell–Boltzmann distribution for energy

$$f(E) = 2\sqrt{\frac{E}{\pi}} \left(\frac{1}{kT}\right)^{3/2} \exp\left(\frac{-E}{kT}\right) \tag{10}$$

and then perform the integral which yields

$$j = \frac{4\pi e m^* k^2}{h^3} T^2 \exp(-q\Phi_{Bn}/kT) \exp(qV/kT) \tag{11}$$

After this, enforce the condition that the current from the metal side to semiconductor side and the semiconductor side to metal side sums to 1: $j = j_{sm} + j_{ms} = 0$ for zero bias (i.e., continuity at 0 V) [6, 1].

1.4 Other Considerations: Ideality Factor and more

The expression for the current density shown in the previous section holds in an ideal case. There are other effects to consider which can affect the IV characteristics.

First, there is the image-charge effect which serves to reduce the barrier height. Electrons from the semiconductor induce charge re-arrangement in the metal, being a conducting surface, such that the system is equivalent to a system with oppositely charged image charges equidistant away from the interface. The image charge exerts an attractive force onto the semiconductor electrons and reduces the amount of energy needed for the electron to overcome the barrier. The current density j is then modified by a factor η called the ideality factor [1, pg. 601]

$$j = j_s \left[\exp\left(\frac{qV}{\eta kT}\right) - 1\right] \tag{12}$$

where $\eta \geq 1$.

Second, the Schottky barrier height is not necessarily homogeneous across the contact area which can lead to the barrier height that we measure to be lower than the mean value of the barrier height. We assume that the barrier height follows a Gaussian distribution so that the Schottky barrier height is modified to be the mean value minus a standard deviation term [1, pg. 603]

$$q\Phi_{Bn} \quad \longrightarrow \quad q\Phi_{Bn} = \langle q\Phi_{Bn} \rangle - \frac{q\sigma^2}{2kT} \tag{13}$$

where again $q\Phi_{Bn}$ are the barrier values that we measure directly using a linearized fit or via the current-voltage data. [1, pg.603]

1.5 Predictions and Existing Data

1. With the metal-semiconductor junction being between a metal and an $n-$type semiconductor, we would expect the IV curve to fit according to the following equation

$$I = Aj_s \left[\exp\left(\frac{qV}{kT}\right) - 1 \right] \tag{14}$$

2. Moreover, existing experimental data give the following plots for the current versus voltage curve for Au-Si, for small applied voltages. We would hope to see similar behavior and current density magnitude.

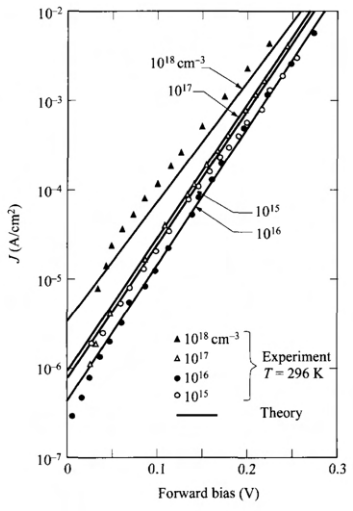

Fig. 19 Theoretical and experimental current-voltage characteristics for Au-Si Schottky barriers. Increased current is due to tunneling. (After Ref. 36.)

Figure 2: Measured and Predicted values Current vs Voltage for Au-Si for various doping concentrations at small voltages [6, pg.163]

3. The work function of gold is $W_m = 4.8\,\text{eV}$ and the electron affinity of the semiconductor is $\chi_{sc} = 4.05\,\text{eV}$. Then, the predicted ideal Schottky barrier height is

$$q\Phi_B = W_m - \chi = (4.8 - 4.05)\,\text{eV} = 0.75\,\text{eV} \tag{15}$$

Other sources give the measured barrier height for Au-Si measured at 300 K to be around 0.83 eV [6, pg. 179]. Though the sample used also has titanium.

2 Procedure

2.1 Preparation: Test Circuit and LabVIEW Programming

We prepared for the measurements in the probe station and PPMS by first constructing the circuit set up below, modifying the provided LabVIEW code to sweep negative voltages, and testing the IV curve measurements with a linear 1 mΩ resistor.

1. Our circuit is illustrated in the figure below where Fig. 3(c) is the test circuit with an ohmic 1 MΩ resistor. The power supplies are connected in series with their polarities reversed which allows us to sweep from negative voltages to positive voltages. In performing the measurements, we only use one channel at once, which reduces the circuit to either Fig. 2(c) or Fig. 3(d) which corresponds to sweeping positive voltages from $(0, V_{\max})$ or sweeping negative voltages from $(-V_{\max}, 0)$.

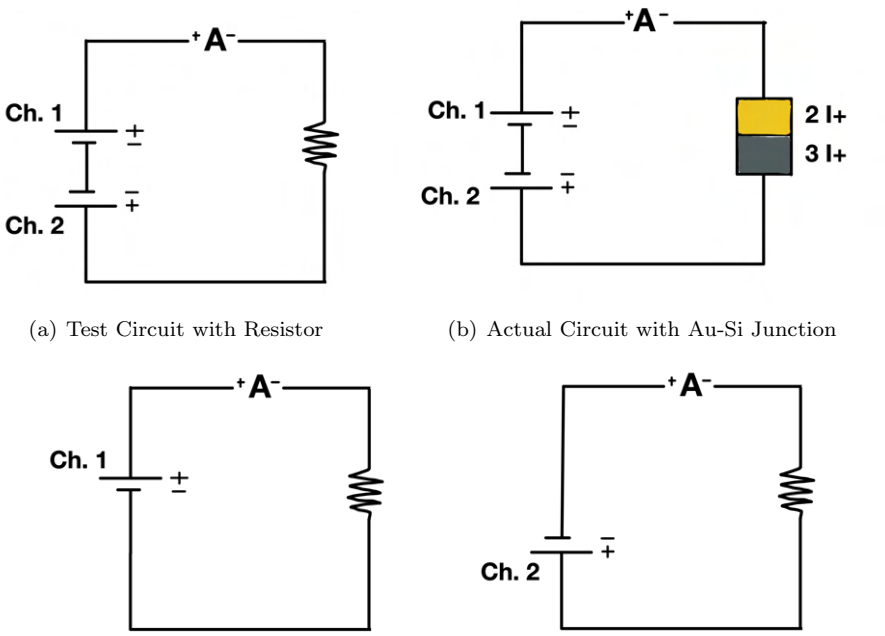

(a) Test Circuit with Resistor

(b) Actual Circuit with Au-Si Junction

(c) Channel 1 Alone

(d) Channel 2 Alone

Figure 3: Schematics of constructed circuits.

2. The test circuit was implemented by using a Keithley 2220G-30-1 Dual Channel DC Power supply in conjunction with a Keithley 2000 multimeter set to measure DC current. We wired the circuit according to the test diagram above using the two channels as separate voltage sources and connected it in series to a 1 MΩ resistor as shown in Fig. 2

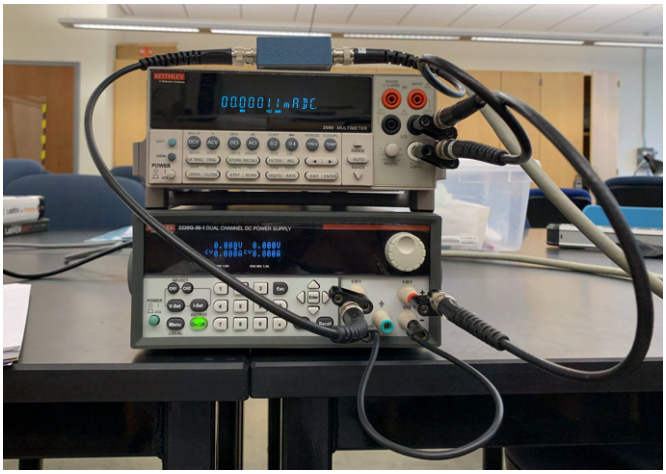

Figure 4: The Implementation - Ch.1 and Ch.2 are wired such that the negative terminals are connected to each other

These instruments are then connected to a computer via a GPIB interfacing port which allows us to control the instruments using a LabVIEW program as discussed in the next section.

3. LabVIEW Code.

We control the instruments remotely using two programs one that controls the positive channel and one that controls the negative channel.

In both cases, we provide the program with the desired maximum voltage $V_{\max}$ and number of iterations n. From that, the program determines the appropriate step size and using a for loop, iterates through increasing the voltage on the power supply by the step size until the maximum voltage has been reached. In the case of the positive channel 1, it begins at $0V$ and increases by $\Delta V = V_{\max}/(n-1)$ until $V_{\max}$ is reached. At each step, the multimeter reads the DC current reading and then writes out the reading to a text file.

In the case of the negative channel code, we took the provided code and modified it to sweep from instead $-V_{\max}$ to 0, which was accomplished by modifying the voltage value passed to start at $V_{\max}$, which is provided by the user, and then subtracting by ΔV at each iteration. Additionally, when it came to writing out the values to the text file, we multiplied the measured voltage and current values by -1 to reflect the fact that we are applying the voltage in the reverse bias direction.

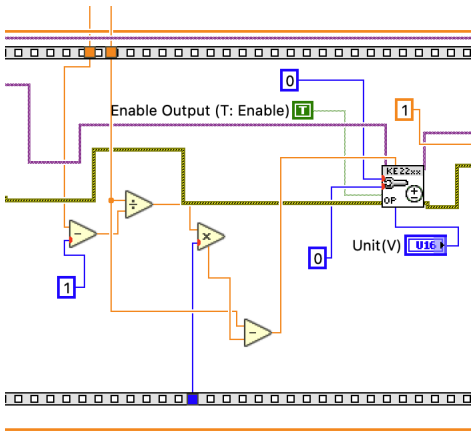

(a) The orange wire that passes from the minus function to the KE22 function passes the voltage value to be used. We pass to the minus function the initial max voltage value (top wire/first argument) and the step size (bottom wire/second argument) so that at each iteration, we are subtracting from the initial max value one ΔV

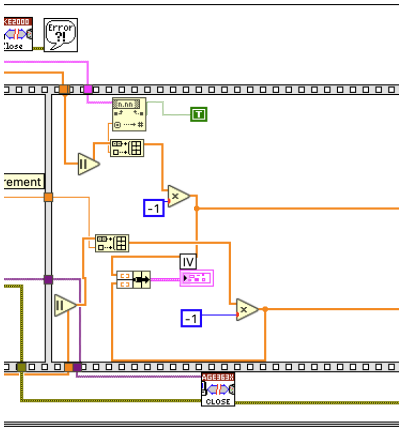

(b) We multiply the outputs by -1 as demonstrated by the multiply functions which take the output from the array generators which hold the measured voltage and current values

Figure 5: Ch. 2 Negative Channel Modifications

2.2 Room Temperature Measurements: Probe Station

In this part, we measure the current as a function of voltage of the Au-Si sample at room temperature using the probe station.

1. The actual metal-semiconductor junction consists of a rectangular undoped silicon wafer of area $0.72\,\mathrm{cm}^2$ upon which gold was deposited such that half of the original area was coated in gold. The substrate was first prepared by cleaning with acetone, methyl alcohol, and finally isopropyl alcohol. The gold is heated and condenses onto the substrate in vacuum to form the thin film using an evaporator.[2]

[2]Thanks to Dr. Ojeda-Aristizabal and the Nanoelectronics lab for preparing the samples for us

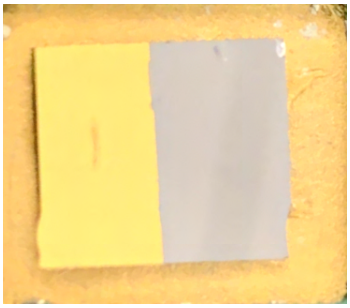

Figure 6: The Au-Si Sample. Half is gold and the grey side is Silicon

2. Using the circuit implementation described in the previous section, that is, using the Keithley multimeter and power supply set up, we place the Au-Si sample into the probe station in place of the ohmic resistor. The probe station consists of a main stage where the sample is placed. Two small probes are lowered to make physical contact, one on the gold side, another on the semiconductor side and are clamped down via vacuum. The probes have leads which feed into the Keithley multimeter and power supply to complete the circuit.

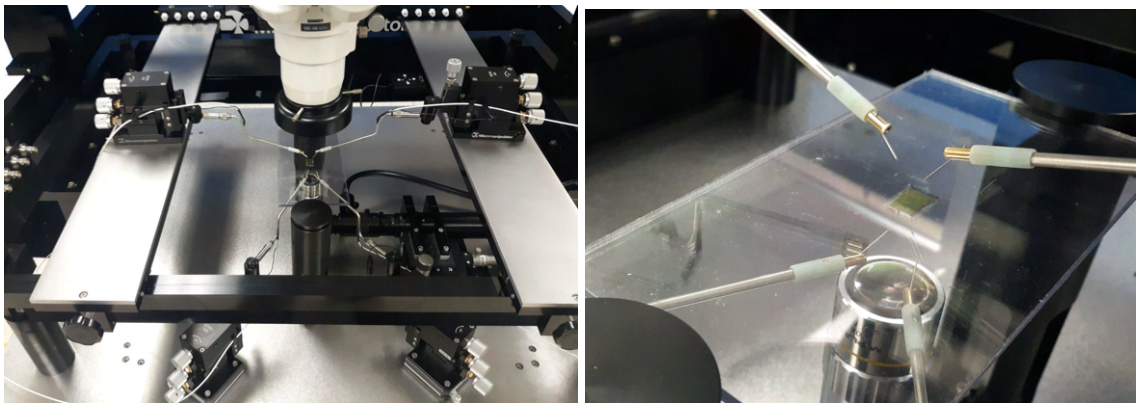

(a) Depiction of a typical Probe Station from Micromanipulator Co. [2]

(b) Up close of the needle-like probes that contact the sample from Micromanipulator Co. Website [3] In our case, we used just two probes, one for the old side and one for the silicon side.

Figure 7: General images of a probe station.

3. We then run the LabVIEW programs, both the positive channel 1 and the negative channel 2, to sweep from -3 V to 3 V and measure the resulting current and store the data values into a CSV file to later be plotted.

2.3 PPMS Measurements

In this part, we use the PPMS which allows for current measurements to be taken while the sample is cooled to lower temperatures thus allowing us to probe the temperature dependence of the current I (in addition to voltage dependence).

1. To start, we[3] wired the Au-Si sample to the PPMS puck, a holder for the sample that allows for the sample to be placed into the PPMS while still being connected to outside instruments. This was done by using annealed gold wire and conductive silver paste. The semiconductor side was connected to node 3 I- and the gold side to node 2 I+ as shown in Fig. 8(a).

[3]Thank you to Derek Bergner and Dr. Ojeda-Aristizabal for helping with the wiring

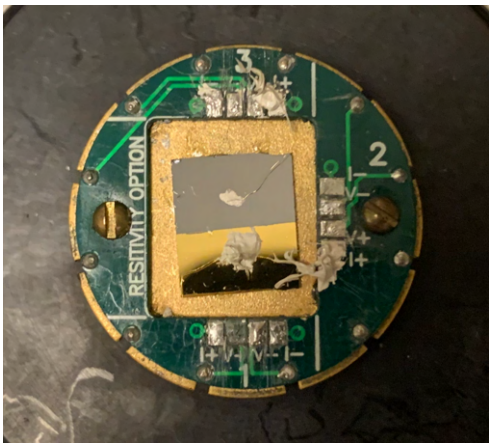

(a) PPMS Puck with Au-Si Sample in the middle and wiring to the semiconductor side at 3 I+ and gold side at 2 I+

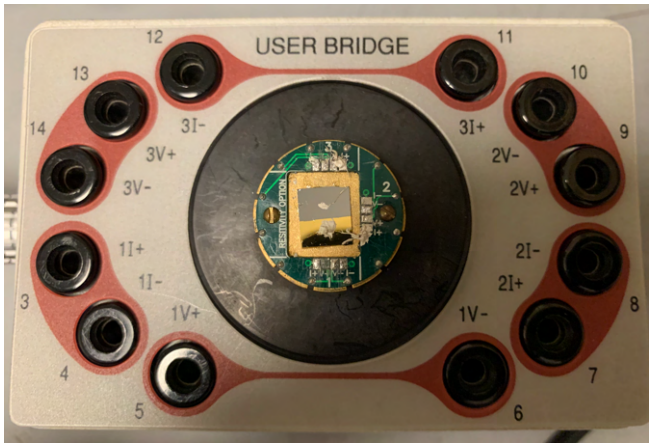

(b) Wiring Test Station with Puck Inside

Figure 8: The Puck and Wiring Test Station

2. Before wiring the sample to the puck, it was necessary to test the connections on the puck to determine the mapping to the BNC connections or labels on the breaker box, which allows connections to the multimeter for current measurement.

   This was done by measuring the resistance of the nodes on the puck while the BNC connections on the breaker box were connected to the multimeter. We hold the breaker box connection fixed and test all the nodes on the puck and record the node that produces non-zero resistance.

   In our case, the mapping was one to one.

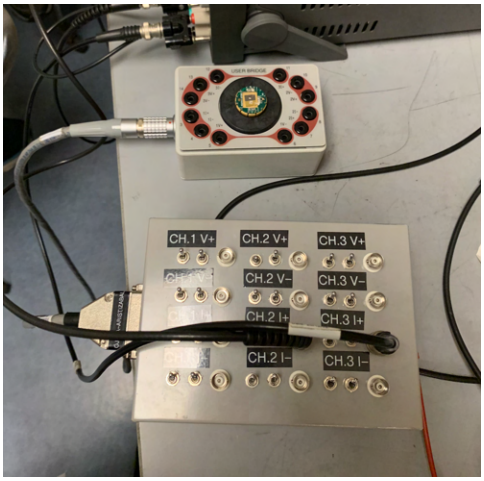

Figure 9: Top: The user bridge/wiring test station where the puck is held. Bottom: The breaker box with corresponding connection labels to which connections to the multimeter and power supply are made

   The connections here are fundamentally different than in the probe station. In the probe station, the circuit was completed by physical probes making contact with the two sides of the sample. Here, the wiring connects the two sides of the sample to nodes on the PPMS puck. In particular, the semiconductor side was connected to 3 I+ and the gold side to 2 I+. The PPMS puck then makes electrical contact to the wiring test station which then is connected to the interfacing box which has the corresponding labels as well as connections for leads from the multimeter and power supply.

3. Then we performed a measurement of the PPMS puck inside of the wiring test station, outside of the

PPMS. As demonstrated in Figure 5, the puck is connected to a breaker box labeled with the relevant channels and corresponding connections. To these connections, we connect leads that lead back to the multimeter and power supply to construct the circuit demonstrated in Figure 2(b).

4. Then, we inserted the puck into the PPMS and we performed a measurement of the PPMS puck at room temperature. To do so, we connected the breaker box to the PPMS using the existing cable[4] that previous fed into the wiring test station. This acts as an intermediary to the puck and the measuring instruments in the same manner as in the wiring test station previously.

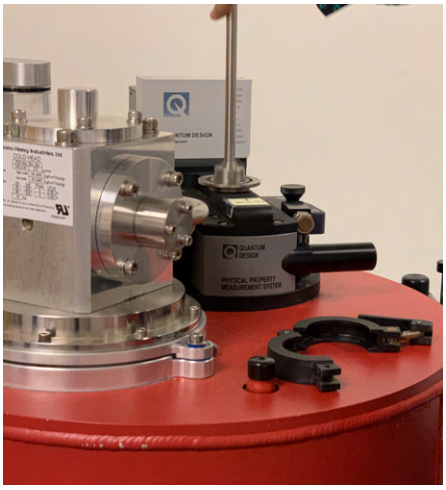

(a) Inserting the puck into the PPMS

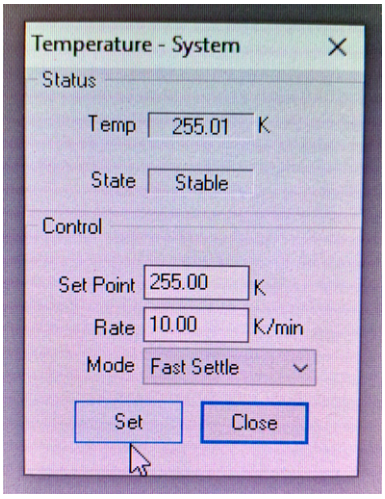

(b) Computer controls for the temperature which indicates state and rate of temperature change

Figure 10: Images of the PPMS Set up

5. After this, we begin to take measurements at varying temperatures. Beginning at 295 K, we then began to decrease the temperatures in increments of 5 K until 275 K. After this, we began to decrease in increments of 10 K until 245 K where we increased to increments of 20 K after 200 K down to a minimum temperature of 20 K. At each measurement, we waited until the PPMS was in the "stable" state before running the Labview code to take the measurement. [5]

3 Results and Data Analysis

3.1 Preparation

When appending the plot data resulting from the circuits in figures 3(c) and 3(d), an issue that we ran into was a discontinuity in the resulting IV plots at the origin where the data from the two channels meet. This was later found to be due to noise and the size of resistor used. We found that even when there was zero voltage applied, the multimeter was still reading about 0.0001 mA or 1×10^{-7} A which led to the offset. At the same time, we were using a 1 MΩ or $1 \times 10^{6}\,\Omega$ resistor and probing from 0 V to 1 V in step sizes of $\Delta V = 0.1$ V so the resulting current measurements were on the order of 10^{-7} A as well which caused the discontinuity at the origin to appear large.

3.2 Room Temperature Results

Below, we have the data plots for the current as a function of voltage for three different cases: the probe station, the sample wiring station, and inside of the PPMS.

[4]Thanks to Derek and Blake for helping remove the existing cable which was extremely stuck
[5]Special thanks to Spencer Halls and the Gu lab for assisting with the PPMS.

We see that in all three cases, the curves qualitatively agree with the expected shape for the Schottky diode. For negative voltages, or a reverse bias, electrons would flow from the metal side to the semiconductor side but face the large barrier and the current is severely restricted. Conversely, for positive voltages, there is no such barrier and the current exhibits the expected exponential curve.

However, one thing to note is the magnitude of the current is much larger for the PPMS and sample wiring test station than for probe station for both the forward and reverse bias, though it is much more dramatic for the forward bias. Though the difference in magnitude is lessened in the reverse bias since in all cases the reverse bias current is much smaller in magnitude than forward bias, we see that the probe station has values much closer to zero than the PPMS and Test station do. A possible explanation is that for the former two cases, the Au-Si sample was wired onto the PPMS puck using silver paste which includes the gold wiring contacting the semiconductor side as well which could have increased the conductivity of the semiconductor. By contrast, in the probe station, the only contact between the semiconductor and the circuit was a physical probe. In this same vein, the contact resistance, the resistance due to surface contact between different objects, for the silver paste and sample is smaller than the contact resistance between the physical probe and the sample which could lead to the greater current magnitude in the PPMS and Test station cases.

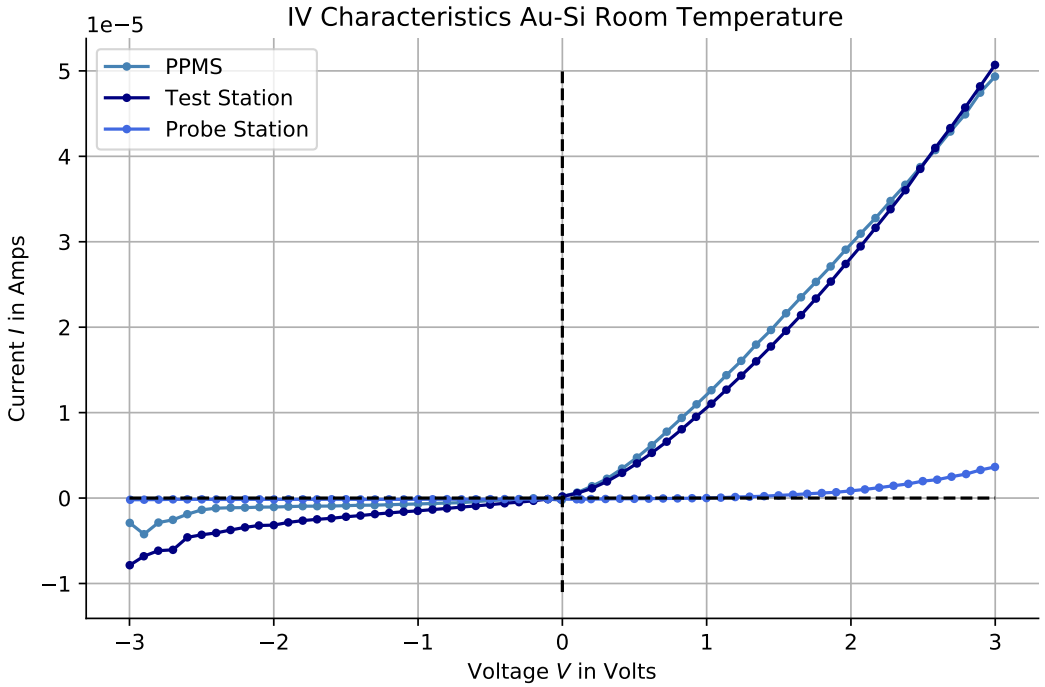

Figure 11: $I(V)$ PPMS, Wiring Test Station, Probe Station Plotted Against Each Other at Room Temperature

3.3 Variable Temperature: PPMS

Below we have the graphs of the current I versus voltage V.

First, we note that at the beginning, as temperatures decreased from 300 K to about 255 K, the magnitude of the current seemed to actually increase. In the reverse bias, towards -5V, we see that there is some non-zero current flow which seems to indicate that around this voltage is the breakdown voltage for this Au-Si Schottky diode.

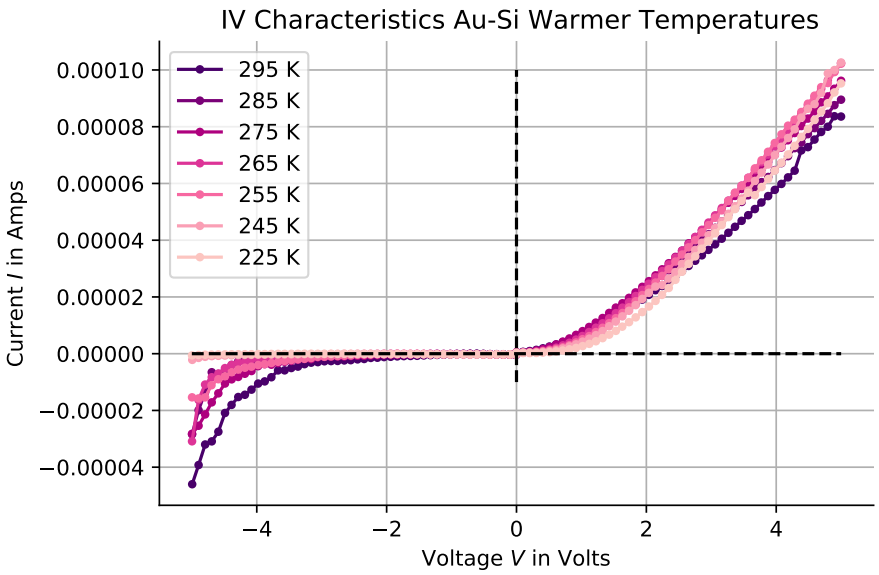

Figure 12: Current dependency on T, V for 225 K to 295 K

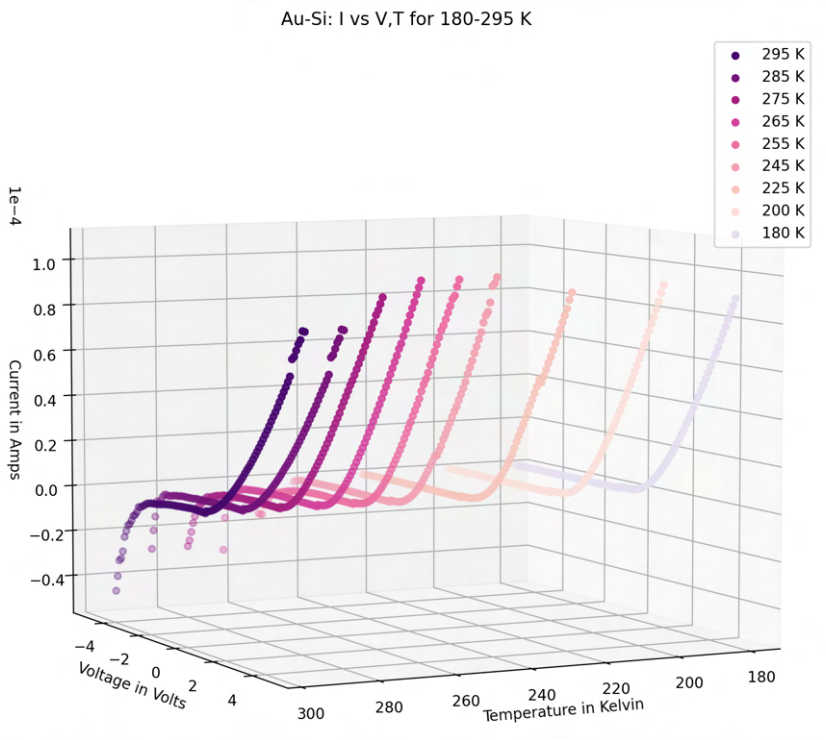

Figure 13: 3D Projection of the data. We can see that the magnitude of the current increases slightly from 295 K to around 245 K after which the magnitude begins to decrease.

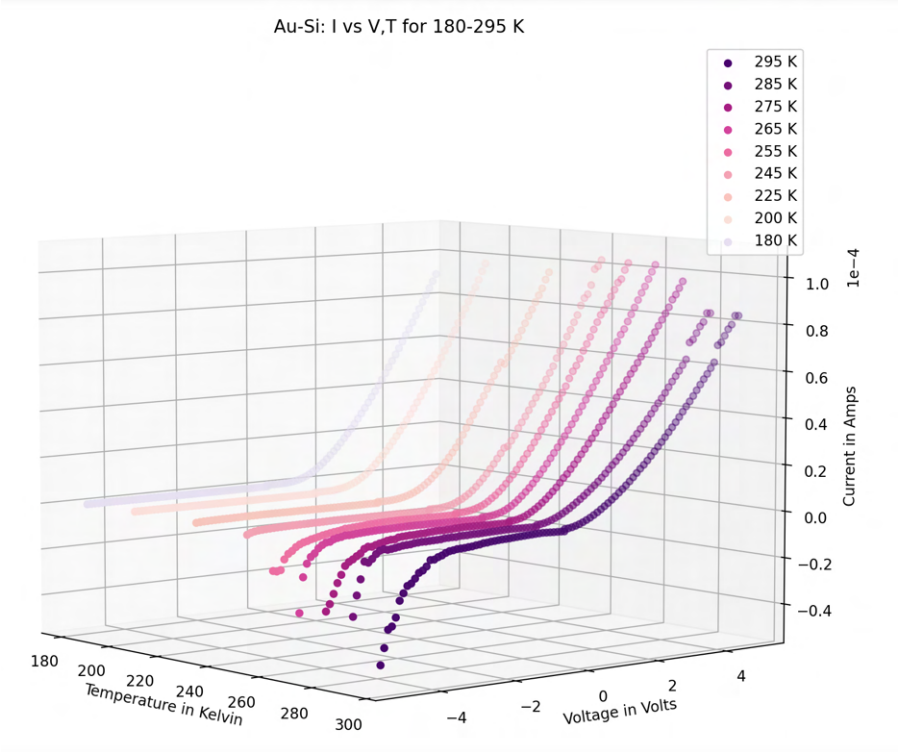

Figure 14: Alternative view. We also see the magnitude of the current in the reverse bias begin to decrease as well as temperature decreases.

However, as temperatures decreased further, the magnitude of the current then seemed to decrease back to the levels at 300 K and then further decrease to eventually being essentially zero at around 20 K with the rate of decrease of the magnitude seemingly increasing as temperature decreases.

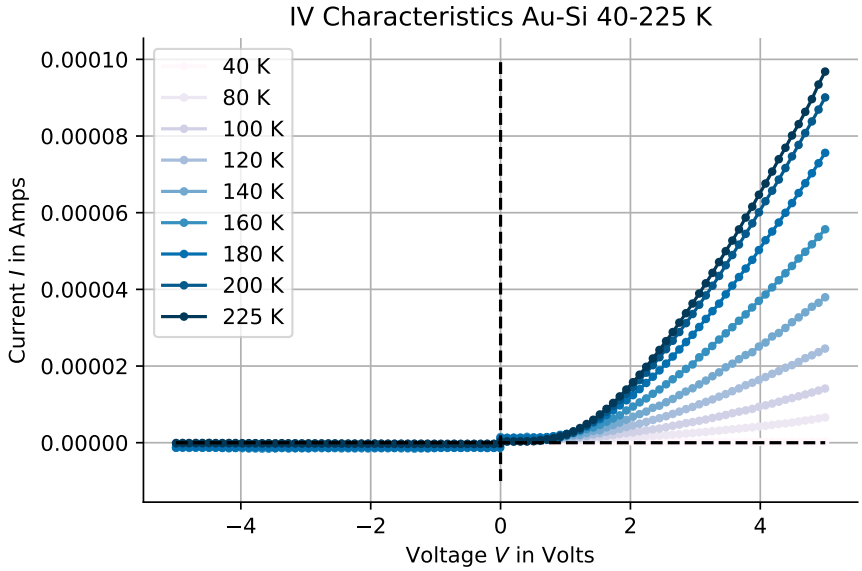

Figure 15: IV Curves from 40 K to 225 K in 20 K increments. As $T \to 0$, the magnitude of the curves decreases

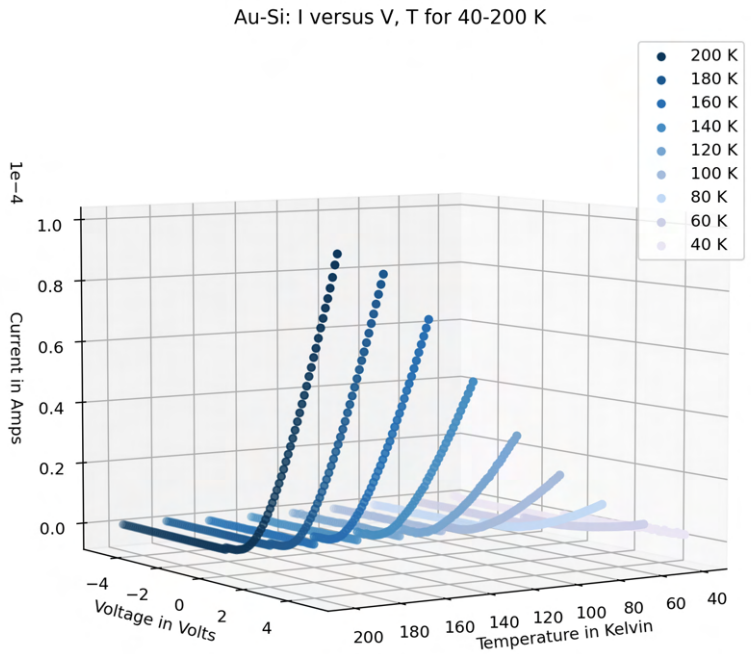

Figure 16: IV curves as a 3D plot of T and V for 40-200 K

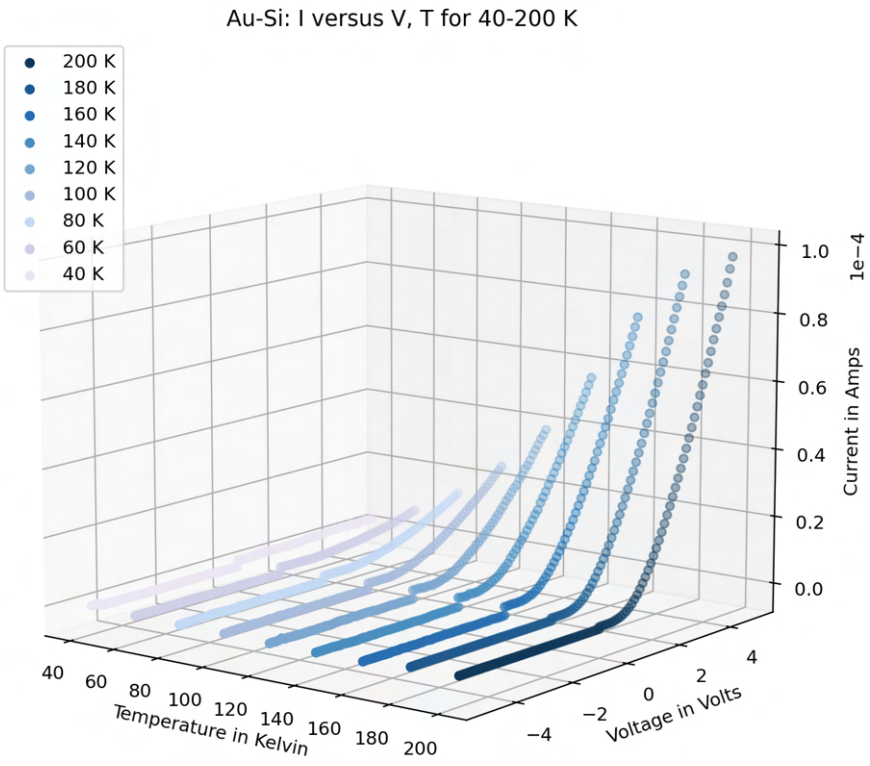

Figure 17: Alternative view of IV curves as a 3D plot of T and V for 40-200 K

Moreover, now that we have sampled the current behavior at different temperatures, we can then slice the

data and examine the temperature dependence on the data for fixed voltages. Doing this from 1 V to 5 V in increments of 1V gives us the following graph in Fig. 18.

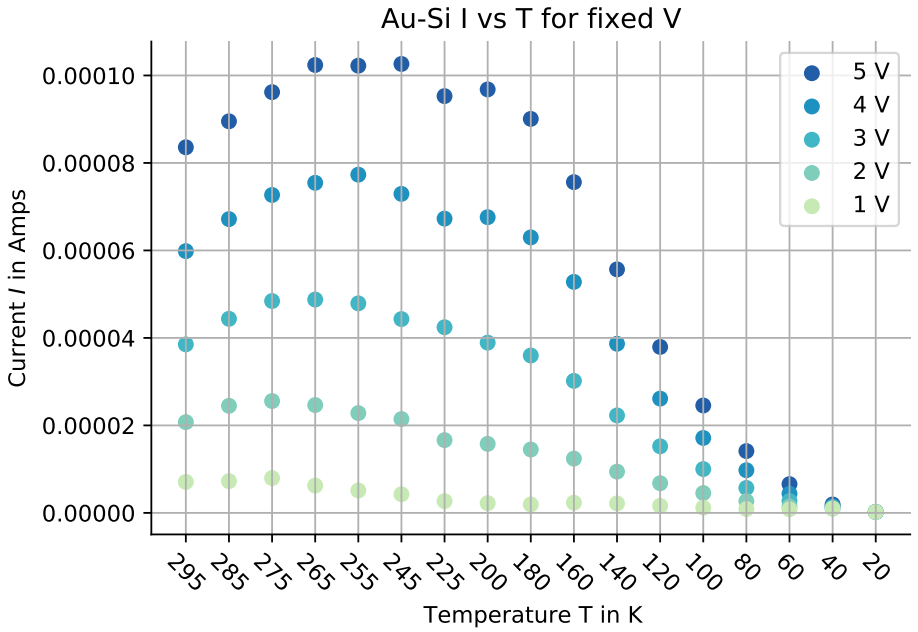

Figure 18: Current as a function of temperature for fixed voltage. We see more clearly the slight increase in current as temperature initially decreases before decreasing at around 245 K.

Repeating this for reverse bias gives us Fig. 19

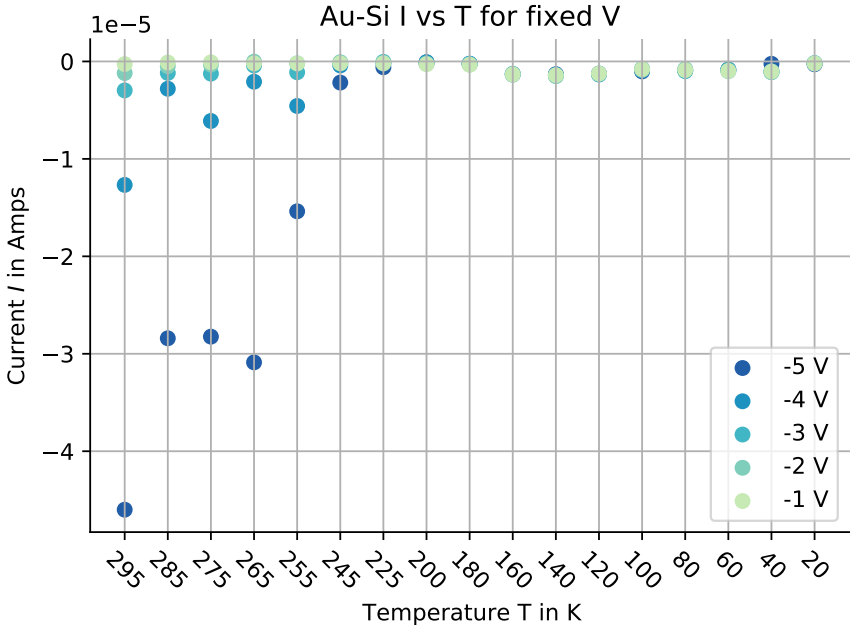

Figure 19: Current as a function of temperature for fixed voltage from $-5V$ to $-1V$

3.4 Analysis

1. **Curve fitting**.

   In this step, we can curve fit the current versus voltage graphs by minimizing the mean square error (MSE) and using a test function of the form below. An alternative fitting method would be to linearize the data by taking the natural log of the current density values and then use a linear fit. However, for our data, we found that subsequent fit was not as good as the MSE method.

   Starting from the following expression for the voltage [6, pg.167]

$$j = j_s \left[\exp\left(\frac{qV}{\eta k_{\mathrm{B}} T} \right) - 1 \right] \tag{16}$$

   and noting that $I = jA$ where $A = 0.72\mathrm{cm}^2$ in for our sample we can use the same general equation to fit I

$$I = I_0 \left[\exp\left(\frac{qV}{\eta k_{\mathrm{B}} T} \right) - 1 \right] \tag{17}$$

   where we need to determine I_0 and $b = q/(\eta k_{\mathrm{B}} T)$. Performing the fit for each temperature, we then have the following table of data. From the fitted I_0, we can then determine j_s by dividing through by $A = 0.72\,\mathrm{cm}^2$.

T (Kelvin)	I_0 (Amps A)	b (inverse Volts V^{-1})	R^2	j_s (A/cm^2)
295	1.8018×10^{-5}	0.3581	0.9455	2.503×10^{-5}
285	1.1945×10^{-5}	0.4523	0.9514	1.659×10^{-5}
275	1.4423×10^{-5}	0.4206	0.9549	2.003×10^{-5}
265	1.1828×10^{-5}	0.4783	0.9551	1.643×10^{-5}
255	1.1899×10^{-5}	0.4773	0.9653	1.6526×10^{-5}
245	8.415×10^{-6}	0.5411	0.9645	1.169×10^{-5}
225	7.6128×10^{-6}	0.5457	0.9598	1.0573×10^{-5}
200	6.7874×10^{-6}	0.5687	0.9691	9.427×10^{-6}
180	6.276×10^{-6}	0.5700	0.9705	8.717×10^{-6}
160	3.948×10^{-6}	0.6140	0.9741	5.483×10^{-6}
140	2.913×10^{-6}	0.6137	0.9724	4.046×10^{-6}
120	2.0104×10^{-6}	0.6110	0.9692	2.792×10^{-6}
100	1.3498×10^{-6}	0.6036	0.9679	1.875×10^{-6}
80	1.6085×10^{-6}	0.4705	0.9893	2.234×10^{-6}
60	1.4407×10^{-6}	0.3444	0.9694	2.001×10^{-6}
40	3.063×10^{-6}	0.1140	0.8204	4.254×10^{-6}
20	-3.531×10^{-6}	-0.0174	0.7388	-4.904×10^{-6}

2. **Saturation Current Density Temperature Dependence, Barrier Height, Richardson Constant**

   From the above section, we then have tabulated data for the saturation current density as a function of temperature. We plot then $j_s(T)$ in Figure 20 where we have removed the 20 K and 40 K data points as the fit for those points, performed in the section above, was not as good as the others.

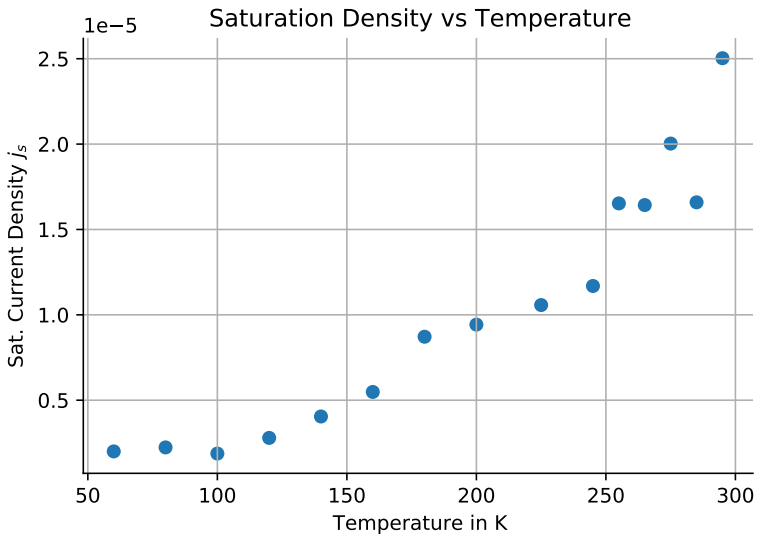

Figure 20: Saturation current density vs temperature. We see that it roughly obeys the same type of dependency as the theoretic expression.

We can compare this to the theoretic expression

$$j_s = A^* T^2 \exp\left(-\frac{\Phi_{Bn}}{kT}\right) \tag{18}$$

and even try a fit of that previous form which should allow us to determine both the effective Richardson constant and the Schottky barrier height Φ_{Bn}. That is, we propose a function

$$j_s = BT^2 \exp\left(-\frac{C}{T}\right) \tag{19}$$

where B, C are fittable parameters. Doing so on these data points yields $B = 2.833 \times 10^{-10}\,\mathrm{Acm^{-2}K^{-2}}$ and $C = 41.1133\,\mathrm{K}$ with $R^2 = 0.9442$, which indicates that the overall behavior of the graph for measured saturation density is consistent with the theoretic expression. On the other hand, the fitted values for the parameters seem to indicate that

$$\boxed{A^* = 2.833 \times 10^{-10} \frac{\mathrm{A}}{\mathrm{cm^2\,K}}} \tag{20}$$

$$\boxed{\Phi_{Bn} = C \cdot k = 41.1133\,\mathrm{K} \cdot (8.617 \times 10^{-5}\,\mathrm{eV\,K^{-1}}) = 0.0035\,\mathrm{eV}} \tag{21}$$

which disagree pretty heavily with typical values with the Richardson constant being off by an order of magnitude of 10^{12}!

3. **Barrier Height via Semi-Log Linear Fit**

For reverse bias, the current-voltage takes the simplified form

$$I = -AA^* T^2 \exp\left(-\frac{q\Phi_{\mathrm{B}}}{kT}\right) \tag{22}$$

We can re-write this as a linearized equation for I/T^2 versus $1/T$ by dividing through by T^2 and then taking the natural logarithm of both sides to get

$$\ln\frac{-I}{T^2} = \ln(AA^*) - \frac{q\Phi_{\mathrm{B}}}{kT} \tag{23}$$

Applying this linearizing scheme for the data points corresponding to reverse bias voltages: $-1, -2, -3, -4, -5V$, we gives us the plot in Fig. 21

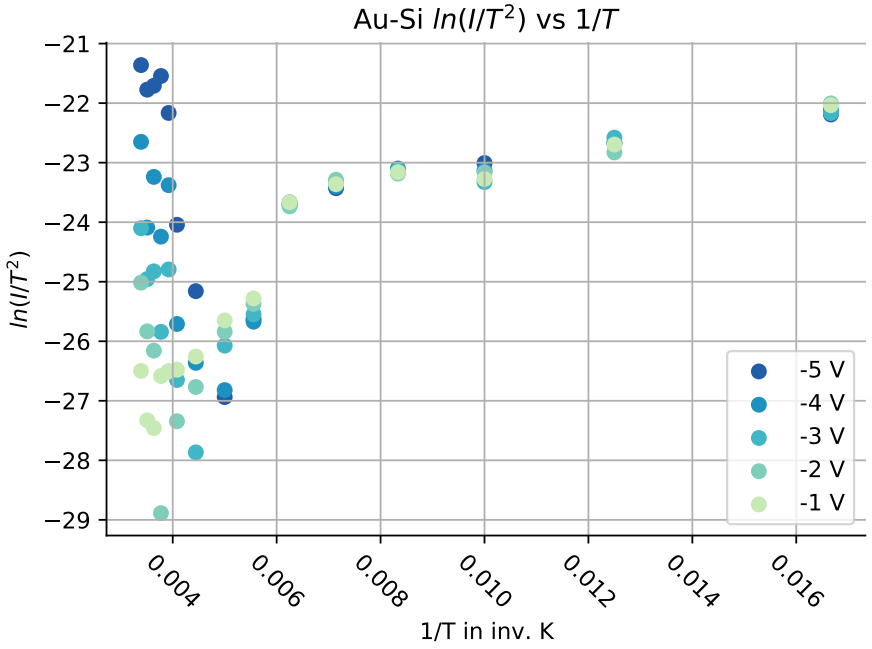

Figure 21: Linearized Dependence

From the data points, we see some interesting behavior as in all cases $\ln\left(I/T^2\right)$ appears to decrease in the range $1/T \in [0.0, 0.005]\,\mathrm{K}^{-1}$ before increasing as $1/T$ increases. From a visual inspection, this data does not permit a good linear fit throughout the entire range. Instead, there are three distinct regions of $1/T$ to fit: $[0.0, 0.005], [0.005, 0.006]$, and $[0.006, 0.016]$. Below, we fit the points corresponding to $[0.0, 0.005]$ which gives us Fig. 22

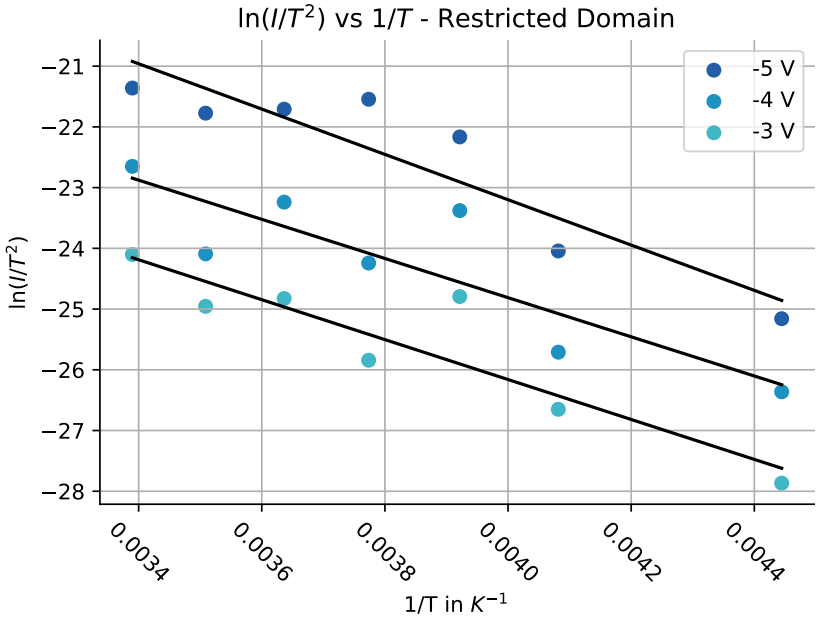

Figure 22: Truncated plot for $1/T$ in 0.0 to 0.005 K^{-1} for -3V, -4V, and -5V data points where the solid black lines are linear fits

The corresponding fitted parameters are given in the table below. Here we also included the fitted parameters for -2V, and -1V which we do not show in Fig. 22 for clarity.

Voltage	Slope m in K^{-1}	Y-Intercept b	$q\Phi_B$ in eV	A^* in $\mathrm{Acm}^{-2}\mathrm{K}^{-2}$
-5V	-3732.0457	-8.2713	0.3216	0.00036
-4V	-3287.2289	-13.0116	0.2779	9.321×10^{-6}
-3V	-3225.1017	-11.9117	0.2833	3.1031×10^{-6}
-2V	-1506.1148	-20.8879	0.1298	1.178×10^{-9}
-1V	759.0290	-29.6314	-0.0654	1.879×10^{-13}

We see that in this case, the values that we get for the barrier height $q\Phi_\mathrm{B}$ is much more agreeable with expected values! (Yay!) However, as the voltage decreases, the barrier height seems to also decrease and we get anomalous results especially for $-2V$ and $-1V$. That being said, we only extracted the barrier height for a very specific interval of data, for a region that looked particularly linear. In fact, the data points that we included consisted only of those measured at temperatures above 225 K. It appears that below these temperatures the data begins to lose its linearity. Which is interesting! Because this might indicate a different type of process becoming more dominant or other parameters that we failed to take into consideration.

4. **Barrier Height Taking into Account Inhomogeneous Barrier Heights.**

Using the expression for the current for reverse bias, we can then, by a similar process in the previous section, solve for the experimentally measured barrier height as a function of temperature T for a given voltage. That is, starting from

$$I = -AA^*T^2 \exp\left(-\frac{q\Phi_B}{kT}\right) \tag{24}$$

for reverse biases, we can solve for $q\Phi_B$ which yields

$$q\Phi_B = -kT \ln \frac{-I}{AA^*T^2} \tag{25}$$

which if we use $A^* = 120\,\mathrm{Amp\,cm^{-2}\,K^{-2}}$, we need only current I as a function of temperature T to get $q\Phi_B$ as a function of temperature (for fixed voltage).

Then the experimentally determined barrier heights $q\Phi_B$ are related to the mean barrier heights $\langle q\Phi_B \rangle$ (at $T = 0K$) [1, pg. 603]

$$q\Phi_B = \langle q\Phi_B \rangle - \frac{\sigma^2}{kT} \tag{26}$$

Performing a linear fit gives us both the standard deviation and the mean barrier height which gives a more accurate representation of the barrier height over the entire edge of the sample as well as the spread. In figure 23 we plot the measured barrier heights as a function of temperature using the method described in equation (25) and see that they are higher than the barriers determined in the previous section, though are still reasonable values being on the same order of magnitude.

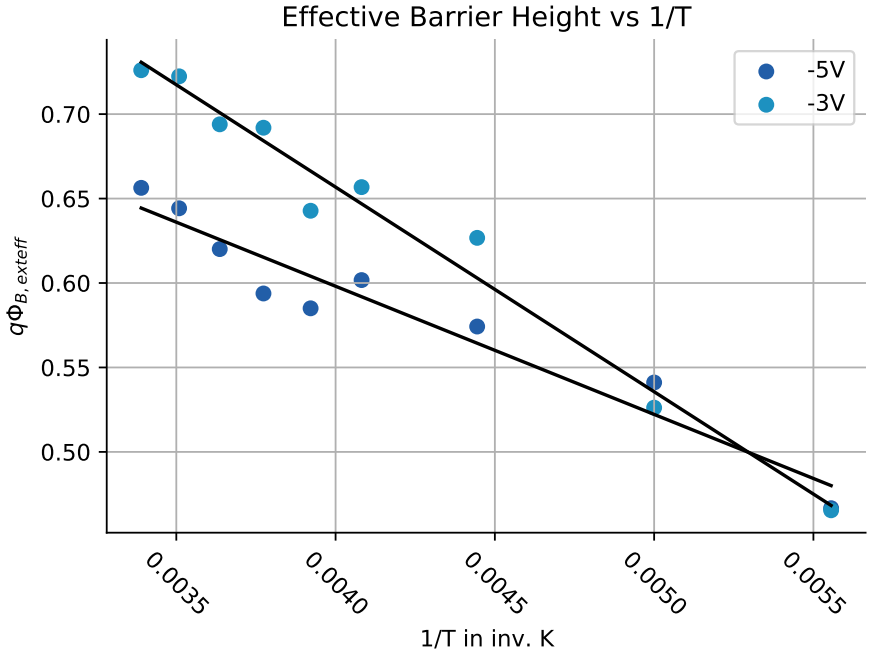

Figure 23: Plot of Barrier Heights versus 1/T along with linear fits (the solid black lines) to determine standard deviation σ^2 and mean barrier height $\langle q\Phi_B \rangle$

The fitted parameters then are

Voltage	Slope m in $\mathrm{K^{-1}}$	Y-Intercept $\langle q\Phi_B \rangle$ in eV	σ^2 in eV^2
-5V	-75.8779	0.9016	6.538×10^{-3}
-4V	-100.5456	1.0340	8.664×10^{-3}
-3V	-121.1685	1.1415	1.044×10^{-2}
-2V	-143.9023	1.2546	1.240×10^{-2}
-1V	-156.7872	1.3102	1.351×10^{-2}

which gives values for the mean barrier height and standard deviation in this model where we assume the barrier heights to be distributed according to a Gaussian distribution.

5. **Ideality Factor**

There are a few possible ways to then extract the dimensionless ideality factor η. From the curve fitting section, we fit the parameter $b = q/(\eta kT)$ to a numerical value. Then, using known values for q, k and T,

we can solve for η

$$\eta = \frac{q}{kTb} \tag{27}$$

Since b has units of inverse volts V we use $k_B = 1.3806 \times 10^{-23}\,\mathrm{J \cdot K^{-1}}$ and $q = 1.602 \times 10^{-19}\,\mathrm{C}$. Doing so via this method gives us the following numerical values for η for a fixed temperature T

Temp K	η
295	109.8420
275	100.3212
265	91.5479
255	95.3373
245	87.5288
225	94.5057
200	102.0191
180	113.0960
160	118.1153
140	135.0549
120	158.2603
100	192.2407
80	308.2798
60	561.5394

which we see are at least larger than unity by a factor of 10^2 which contrasts with typical values for $\eta \sim 1$ as well.

4 Conclusions

To recap, the purpose of this experiment was to explore the characteristics of a Schottky diode and in particular measure the current I as a function of voltage V and temperature T as well as become acquainted with LabVIEW and experimental techniques such as wiring [6] and working with a closed cycle cryostat.

Overall, our measurements of the current followed the general trends expected for a Schottky diode: we see the overall decrease in current magnitude as temperature decreases for both reverse and forward bias as well as the current dependency on voltage for fixed temperature obeying the relation predicted by thermal emission theory in equation 11 as demonstrated in the graphs in the Data Analysis section.

Moreover, from the measured data, we were able to extract various quantities of interest such as the Schottky Barrier height $q\Phi_B$, the ideality factor η, and Richardson constant A^*. From analyzing the reverse-bias current and fitting to a linearized version of the current dependency on voltage, we find values for the Schottky Barrier height that are on the same order of magnitude as the theoretical predicted value. Additionally, repeating this via a second method which takes into account the possibility of barrier inhomogeneity, leads to barrier heights on the same order of magnitude as the previous method, albiet with higher values.

Despite the successes described above, there were nonetheless a few anomalies. In extracting the barrier height via the semi-log linear fit, we see that the heights appear to have a voltage dependence, increasing as the magnitude of the voltage increases which is something that is not present in the ideal Schottky diode case. Additionally, our measured values for the Richardson constant and ideality factors were orders of magnitude off of the predicted values. Moreover, the order of magnitude of the current was significantly smaller than theoretical predictions as well. One possible area of consideration is that the silicon substrate was undoped. The theoretic expressions provided in the introduction were calculated in the case of a metal-semiconductor junction for an $n-$typed doped semiconductor for typical doping concentrations of around 10^{13} - $10^{15}\,\mathrm{cm^{-3}}$ whereas the number density of free electrons in undoped silicon is around $10^{10}\,\mathrm{cm^{-3}}$. With a higher doping concentration, the magnitude of the current could be be much larger. As observed in Fig. 2, the magnitude of the $J(V)$ curve increased for higher doping concentrations where the doping was on the order of 10^{15} - $10^{18}\,\mathrm{cm^{-3}}$. Moreover, for some of the plots where we expected a linear fit throughout the range, we instead see highly nonlinear behavior

[6] And hopefully build character and become better people along the way

which perhaps indicates different physics that we did not take into account, which is interesting! In the future, were we to do this again, we could consider additional modifications to the standard thermal emission theory such as additional transport methods or other modifications a kin to the inhomogeneous barrier heights that we used in the data analysis section.

References

[1] Grundmann, M., *The Physics of Semiconductors - An Introduction Including Nanophysics and Applications 3rd edition* (Springer International, Switzerland, 2016).

[2] Micromanipulator,, "Probe station," `https://micromanipulator.com/wp-content/uploads/2016/10/VERSA-double-sided-prober-front-view-updated.jpg` (2021), 09-28-2021.

[3] Micromanipulator,, "Probe station 2," `https://micromanipulator.com/wp-content/uploads/2016/10/VERSA-double-sided-prober-close-up-from-top--scaled.jpg` (2021), 09-28-2021.

[4] Misra, P. K., *Physics of Condensed Matter* (Acaemic Press, Elsevier, 2012).

[5] Simon, S. H., *The Oxford Solid State Basics* (Oxford University Press, Oxford, United Kingdom, 2013).

[6] Sze, S. and Ng, K. k., *Physics of Semiconductor Devices 3rd edition* (Wiley-Interscience - John Wiley and Sons., Hoboken, New Jersey, 2006).